



This discussion paper is/has been under review for the journal Atmospheric Chemistry and Physics (ACP). Please refer to the corresponding final paper in ACP if available.

Trends in Peroxyacetyl Nitrate (PAN) in the upper troposphere and lower stratosphere over Southern Asia during the summer monsoon season: regional impacts

S. Fadnavis¹, M. G. Schultz², K. Semeniuk³, A. S. Mahajan¹, L. Pozzoli⁴,
S. Sonbawane¹, S. D. Ghude¹, M. Kiefer⁵, and E. Eckert⁵

¹Indian Institute of Tropical Meteorology, Pune, India

²Department of Earth and Space Sciences and Engineering, York University, Toronto, Canada

³Institute for Energy and Climate Research-Troposphere (IEK-8), Forschungszentrum Jülich, Jülich, Germany

⁴Eurasia Institute of Earth Sciences, Istanbul Technical University, Turkey

⁵Karlsruhe Institute of Technology, Institute for Meteorology and Climate Research, Karlsruhe, Germany

Regional impacts

S. Fadnavis et al.

Title Page

Abstract

Introduction

Conclusions

References

Tables

Figures



Back

Close

Full Screen / Esc

Printer-friendly Version

Interactive Discussion



Received: 18 June 2014 – Accepted: 9 July 2014 – Published: 22 July 2014

Correspondence to: S. Fadnavis (suvarna@tropmet.res.in)

Published by Copernicus Publications on behalf of the European Geosciences Union.

ACPD

14, 19055–19094, 2014

Regional impacts

S. Fadnavis et al.

Title Page

Abstract

Introduction

Conclusions

References

Tables

Figures



Back

Close

Full Screen / Esc

Printer-friendly Version

Interactive Discussion



Abstract

We analyze temporal trends of Peroxyacetyl Nitrate (PAN) retrievals from the Michelson Interferometer for Passive Atmospheric Sounding (MIPAS) during 2002–2011 in the altitude range 8–23 km over the Asian summer monsoon (ASM) region. The greatest enhancements of PAN mixing ratios in the upper troposphere and lower stratosphere (UTLS) are seen during the summer monsoon season from June to September. During the monsoon season, the mole fractions of PAN show statistically significant (at 2 sigma level) positive trends from 0.2 ± 0.05 to 4.6 ± 3.1 ppt year⁻¹ (except between 12–14 km) which is higher than the annual mean trends of 0.1 ± 0.05 to 2.7 ± 0.8 ppt year⁻¹. These rising concentrations point to increasing NO_x (= NO + NO₂) and volatile organic compound (VOC) emissions from developing nations in Asia, notably India and China.

We analyze the influence of monsoon convection on the distribution of PAN in UTLS with simulations using the global chemistry-climate model ECHAM5-HAMMOZ. During the monsoon, transport into the UTLS over the Asian region primarily occurs from two convective zones, one extending from the Bay of Bengal to the South China Sea and the other over the southern flank of the Himalayas.

India and China are NO_x limited regions, and thus we use the model to evaluate the contributions from enhanced NO_x emissions to the changes in PAN, HNO₃ and O₃ concentrations in the UTLS. From a set of sensitivity experiments with emission changes in particular regions it can be concluded that Chinese emissions have a greater impact on the concentrations of these species than Indian emissions. NO_x emissions increases over India are about half of those over China.

1 Introduction

One of the intriguing aspects of the boreal summer monsoon circulation, which is active over the polluted land mass of Asia, is venting of chemical constituents from the boundary layer and their redistribution in the Upper Troposphere and Lower Strato-

Title Page

Abstract

Introduction

Conclusions

References

Tables

Figures



Back

Close

Full Screen / Esc

Printer-friendly Version

Interactive Discussion



Regional impacts

S. Fadnavis et al.

Title Page

Abstract

Introduction

Conclusions

References

Tables

Figures



Back

Close

Full Screen / Esc

Printer-friendly Version

Interactive Discussion



sphere (UTLS) (Gettelman et al., 2004; Park et al., 2004, 2007; Li et al., 2005; Randel and Park, 2006; Fu et al., 2006; Xiong et al., 2009; Randel et al., 2010; Fadnavis et al., 2013). The redistributed chemical constituents in the UTLS influence the radiative balance and heat transport in the atmosphere (Ravishankara, 2012; Fadnavis et al., 2013).

For example monsoon injection contributes $\sim 75\%$ of the total net upward water vapor flux in the tropics at tropopause levels (Gettelman et al., 2004). The increased amount of water vapor in the lower stratosphere could enhance ozone depletion and thus raise ultraviolet radiation levels at Earth's surface (Anderson et al., 2012). Satellite observations show convective transport and mixing of chemical constituents, (e.g. aerosols, CO, NO_x, CH₄ and HCN) in the tropical tropopause region during the Asian Summer Monsoon (ASM) season (Dodion et al., 2008; Park et al., 2009; Randel et al., 2010; Vernier et al., 2011). In the stratosphere, these chemical constituents are transported to southern subtropics by the Brewer Dobson circulation (Park et al., 2004; Fadnavis et al., 2013) and they affect ozone, water vapour and aerosol-related constituents in the global stratosphere (Randel et al., 2010; Randel and Jensen, 2013). Peroxyacetyl nitrate (PAN) is one of such chemical species that is important in the tropical UTLS over the south Asian regions for three reasons: (1) It is a secondary pollutant with implications for the production of tropospheric ozone (O₃), (2) PAN is also a useful tracer for diagnosing transport due to monsoon convection and understand redistribution of NO_x in the global stratosphere, (3) In the lower stratosphere PAN releases NO_x which contributes to ozone destruction (Singh and Hanst, 1981; Singh et al., 1986; Sillman and Samson, 1995; Schultz et al., 1999).

PAN mixing ratios vary from less than 1 pptv in the remote marine atmosphere (as observed in NASA GTE PEM-Tropics B campaign in the South Pacific lower marine boundary layer, data available at <http://acd.ucar.edu/~emmons/DATACOMP/>) to several ppbv in the polluted urban environment and biomass burning plumes (Ridley et al., 1992; Singh et al., 1998). In the UTLS mixing ratios are typically in the range 10–300 pptv (Emmons et al., 2000; Keim et al., 2008). PAN is formed exclusively from the chemical reaction of peroxyacetyl radicals (CH₃C(O)OO) with NO₂. The peroxyacetyl

Regional impacts

S. Fadnavis et al.

Title Page

Abstract

Introduction

Conclusions

References

Tables

Figures

◀

▶

◀

▶

Back

Close

Full Screen / Esc

Printer-friendly Version

Interactive Discussion



radical is generated from the oxidation of acetaldehyde (CH_3CHO) by OH, or through photolytic decomposition of acetone (CH_3COCH_3) and methylglyoxal (CH_3COCHO), which are secondary pollutants, produced by oxidation of other NMVOCs such as propene (C_3H_6). In the upper troposphere photolysis of acetone (CH_3COCH_3) is an important source of peroxyacetyl radicals (Fischer et al., 2013). The main loss reactions of PAN are thermal decomposition (most important in the lower troposphere up to ~ 500 hPa), photolysis (most important in the UTLS and above), and the reaction with OH. All of these reactions lead to the formation of reactive nitrogen compounds: the first two reactions yield NO_2 , while the reaction with OH yields NO_3 as a product. At the surface, PAN can also be deposited. Its dry deposition velocity is on the order of 0.5 cm s^{-1} during day time and 0.1 cm s^{-1} during night time (Wu et al., 2012).

Rapid industrialization, traffic growth and urbanization in Asia cause increasing emissions of ozone precursors including NO_x and VOCs. These emissions are projected to increase through 2020 in spite of the efforts of Asian countries to combat air pollution problems (Ohara et al., 2007). Most parts of Asia are NO_x limited regions, i.e. controlling NO_x in these regions would reduce ozone concentrations (Yamaji et al., 2006; Sinha et al., 2013). India and China are by far the largest emitters in Asia. Satellite observations by the SCanning Imaging Absorption SpectroMeter for Atmospheric CHartography (SCIAMACHY) and Ozone Monitoring Instrument (OMI) exhibit positive trends $\sim 3.8 \text{ \% year}^{-1}$ in tropospheric column NO_2 over India (Ghude et al., 2013) and $7.3(\pm 3.1) \text{ \% year}^{-1}$ over China (Schneider and van der A, 2012). Although there is a debate if these observed NO_x changes can be directly related to emission changes, there is no doubt that increased NO_x concentrations may enhance the formation of PAN, some of which is then transported into the UTLS by the Asian summer monsoon (ASM) circulation. In addition to PAN being transported from the polluted boundary layer it can also be formed in the upper troposphere through the production of NO_x from lightning (Tie et al., 2001; Zhao et al., 2009). Lightning activity over Southern Asia is highest during the monsoon season (Ranalkar and Chaudhari, 2009; Penki and Kamra, 2013). The estimated global NO_x production by lightning is $\sim 3 \text{ Tg N yr}^{-1}$ (Nesbitt et al., 2000;

Tie et al., 2002). Simulations with the model of ozone and related tracers (MOZART) show an increase in UTLS PAN over the ASM region due to lightning by 20–30 % (Tie et al., 2001).

Thus it is interesting to examine the influence of Asian monsoon convection on the distribution of PAN in the global UTLS. Also, the impact of enhanced NO_x emissions from India and China, on the redistribution of PAN and other related chemical species, in the global UTLS merits attention. For this we employ the state-of-the-art ECHAM5-HAMMOZ chemistry climate model (Roeckner et al., 2003; Horowitz et al., 2003; Stier et al., 2005). We perform sensitivity simulations in order to investigate the relative contributions from India and China to the increased UTLS PAN concentrations. The paper is organized as follows: data analysis, model description and setup are described in Sect. 2. In Sect. 3, we discuss the distribution of PAN in the UTLS during the ASM from satellite measurements and its transport from model simulations. Section 4 contains satellite observed trends in PAN over the south Asian countries India and China. The impact of enhanced anthropogenic Asian NO_x on PAN, HNO_3 and ozone are discussed in Sect. 5. Conclusions are given in Sect. 6.

2 Data and analysis

2.1 Satellite measurement

The MIPAS–E instrument onboard the ENVironmental SATellite (ENVISAT) was launched in March 2002 into a polar orbit of 800 km altitude, with an orbital period of about 100 min and an orbit repeat cycle of 35 days. MIPAS–E (Fischer and Oelhaf, 1996; Fischer et al., 2008) was a Fourier Transform Spectrometer that provided continual limb emission measurements in the mid infrared over the range $685\text{--}2410\text{ cm}^{-1}$ ($14.6\text{--}4.15\text{ }\mu\text{m}$). From June 2002 to March 2004 MIPAS operated in its full spectral resolution mode at an unapodized resolution of 0.035 cm^{-1} , and with tangent altitude steps of 3 km in the UTLS. From January 2005 through the end of the mission the spectral

Regional impacts

S. Fadnavis et al.

Title Page

Abstract

Introduction

Conclusions

References

Tables

Figures

◀

▶

◀

▶

Back

Close

Full Screen / Esc

Printer-friendly Version

Interactive Discussion



Regional impacts

S. Fadnavis et al.

Title Page

Abstract

Introduction

Conclusions

References

Tables

Figures



Back

Close

Full Screen / Esc

Printer-friendly Version

Interactive Discussion



resolution was reduced to 0.0875 cm^{-1} , while the tangent altitude steps in the UTLS were reduced to 1.5–2 km. Until the platform's failure in April 2012 MIPAS monitored atmospheric minor constituents affecting atmospheric chemistry including PAN, NO_x , and O_3 . The details of the general retrieval method and setup, error estimates and use of averaging kernel and visibility flag are documented by von Clarmann et al. (2009). Details of the PAN retrievals, error budget, and vertical resolution are given by Glatthor et al. (2007) for the 2002–2004, and by Wiegele et al. (2012) for the 2005–2012 measurement period.

In this study we analyze the MIPAS-E observed PAN data during the period 2002–2011. The data is archived from http://share.lsd.fkit.edu/imk/asf/sat/mipas-export/Data_by_Target/. The data versions used are V3O_PAN_5 for 2002–2004, and V5R_PAN_220/V5R_PAN_221 for 2005–2011. The data is processed as per the quality specifications given in the documentation. The useful height range is specified as 5 to 23 km. The data are contoured and gridded at 4° longitude and 8° latitude resolution.

2.2 ECHAM5-HAMMOZ model simulation and experimental setup

The ECHAM5-HAMMOZ aerosol-chemistry-climate model used in the present study comprises of the general circulation model ECHAM5 (Roeckner et al., 2003), the tropospheric chemistry module, MOZ (Horowitz et al., 2003), and the aerosol module, Hamburg Aerosol Model (HAM) (Stier et al., 2005). The gas phase chemistry is based on MOZART-2 model (Horowitz et al., 2003) chemical scheme, which includes a detailed chemistry of O_x - NO_x -hydrocarbons with 63 tracers and 168 reactions. The O_1D quenching reaction rates were updated according to Sander et al. (2003), and isoprene nitrates chemistry according to Fiore et al. (2005). In the MOZART chemical mechanism the PAN formation process occurs through the reaction of Peroxy Acetyl radical (CH_3CO_3) and NO_2 . This reaction is reversible and the thermal decomposition of PAN back to CH_3CO_3 and NO_2 is the main sink of PAN. The reaction rates for this reversible reaction are updated according to Sander et al. (2006). CH_3CO_3 is mainly formed

Regional impacts

S. Fadnavis et al.

Title Page

Abstract

Introduction

Conclusions

References

Tables

Figures



Back

Close

Full Screen / Esc

Printer-friendly Version

Interactive Discussion



by oxidation of acetaldehyde (CH_3CHO) by OH, and by the photolytic decomposition of Acetone (CH_3COCH_3) and Methylglyoxal (CH_3COCHO). In the model simulations we included emissions of acetone from anthropogenic sources and wild fires (primary sources), while acetaldehyde and methylglyoxal are produced by oxidation of other NMVOCs (secondary sources). In particular oxidation of primary NMVOCs like ethane (C_2H_6), propane (C_3H_8) and propene (C_3H_6) forms acetaldehyde, while CH_3COCHO is mainly formed from the oxidation products of isoprene and terpenes. Higher Acyl Peroxy Nitrates (MPAN) are included in MOZART-2 chemical scheme, they are also formed through oxidation of NMVOCs, but their production is not significant compared to PAN. The main loss process of PAN from the atmosphere is the thermal decomposition into its precursors. Other loss processes are photolysis and reaction with OH. In ECHAM5-HAMMOZ dry deposition follows the scheme of Ganzeveld and Lelieveld (1995). Soluble trace gases such as HNO_3 and SO_2 are also subject to wet deposition. In-cloud and below cloud scavenging follows the scheme described by Stier et al. (2005). PAN is not highly water soluble, therefore wet deposition is a minor removal process, and dry deposition is also not significant.

The model is run at a spectral resolution of T42 corresponding to about $2.8^\circ \times 2.8^\circ$ in the horizontal dimension and 31 vertical hybrid σ - p levels from the surface up to 10 hPa. The details of model parameterizations, emissions and validation are described by Fadnavis et al. (2013), Pozzoli et al. (2008a, b, 2011). Here, we note that our base year for aerosol and trace gas emissions is 2000. Each member of our sensitivity study consists of continuous simulations for 10 years from 1995 to 2004. Emissions were the same in each simulation, and meteorology varied because of different sea surface temperature (SST) and sea ice (SIC) data. The AMIP2 SSTs and SIC representative of the period 1995–2004 were specified as a lower boundary condition.

In order to understand the impact of enhanced anthropogenic NO_x emissions on the distributions of PAN, HNO_3 and ozone in the UTLS, we conducted 6 simulations for the period 1995–2004: (1) a reference experiment and five sensitivity experiments (refer 2–6) where NO_x emissions over India and China were scaled according to the

Regional impacts

S. Fadnavis et al.

Title Page

Abstract

Introduction

Conclusions

References

Tables

Figures



Back

Close

Full Screen / Esc

Printer-friendly Version

Interactive Discussion



observed trends. Simulation (2) increases NO_x emissions over India by 38 % (Ind38), run (3) those over China by 73 % (Chin73). Experiment (4) shows the effect of the combined changes (India by 38 %, China by 73 %) (Ind38Chin73). Experiment (5) assumes equal relative changes of NO_x emissions (India by 38 %, China by 38 % (Ind38Chin38)) in order to analyze the respective contributions, and to understand the regional emission enhancement impact on the UTLS for same emission enhancement over China, in experiment (6) emissions are increased over India by 73 % (Ind73). The emission perturbations were derived from observed NO_2 trends of $\sim 3.8 \text{ \% year}^{-1}$ over India (Ghude et al., 2013) and $7.3 (\pm 3.1) \text{ \% year}^{-1}$ over China (Schneider and van der A, 2012). Similar values of NO_2 trends ($5\text{--}10 \text{ \% year}^{-1}$) are also reported by Hilboll et al. (2013) over the megacities of India and China.

3 Results and discussions

3.1 Comparison with aircraft measurements

Model simulated PAN, NO_x , HNO_3 and Ozone mixing ratios are evaluated with climatological datasets of airborne campaigns during the monsoon season (June–September). The data were retrieved from <http://acd.ucar.edu/~emmons/DATACOMP/CAMPAIGNS/>. The NO_x and ozone volume mixing ratios observed during CAIPEEX experiment, September 2010, are evaluated over the Indian region. The details of instrument and measurement technique are available at <http://www.tropmet.res.in/~caipeex/about-data.php>. The list of data sets and aircraft campaigns are presented in Table 1. For the comparison, aircraft observations are averaged over 0–2 km, 2–6 km and 6–8 km and at the center latitude and longitude of the flight region. Model simulations are also averaged at the same altitudes. Figure 1a–k compare the observed global distribution of PAN, ozone, HNO_3 and NO_x to those simulated by ECHAM5-HAMMOZ. The mean aircraft observations are shown as filled circles and model output are background contours. Figure 1 indicates that model simulated PAN, HNO_3 and NO_x show

good agreement with aircraft measurements. Ozone, however, exhibits a low bias over south America (for 0–6 km). In the upper troposphere (6–10 km) model simulated ozone shows better comparison (than lower troposphere) with aircraft observations. HNO₃ shows lower values in the Atlantic, west of Africa and Ireland, for 2–6 km and 6–10 km.

5 Model simulated ozone and NO_x show good agreement with CAIPEEX measurements over the Indian region.

3.2 Transport of PAN into the UTLS due to monsoon convection

Figure 2a shows the vertical variation during the annual cycle of the MIPAS-E PAN climatology (for the period 2002–2011) averaged over the ASM region (10–40° N; 60–120° E). ECHAM5-HAMMOZ simulated PAN mole fractions are smoothed with the averaging kernel of MIPAS. The monthly distribution clearly shows elevated levels of PAN in the UTLS during the ASM season (June–September). Seasonal variation of ECHAM5-HAMMOZ simulated PAN (obtained from reference experiment) over this region is plotted in Fig. 2b for comparison. It also indicates plume rising into the UTLS during the ASM season, although PAN mole fractions are less than those obtained from MIPAS-E especially during July and August. These differences may be due to uncertainties in VOC emissions and chemistry represented in the model. Also MIPAS-E views the atmosphere from above and there are uncertainties in the MIPAS-E retrievals. The comparison of cross-section plots (not included) of MIPAS-E PAN with model simulated PAN indicate that in the UTLS (8–23 km), MIPAS-E PAN is higher than model simulated PAN by ~ 20–60 ppt. It is lower by 20–40 ppt over eastern part of anticyclone and 40–50 ppt over Indonesia northern Australia. Near the southern pole MIPAS-E is PAN higher than ECHAM5-HAMMOZ by 70–90 ppt. The model could not produce high PAN concentrations near the southern pole between 17 and 23 km. In the ASM region during the monsoon season MIPAS-E PAN is higher than model by 30–60 ppt. The comparison of PAN measurements from MIPAS-E with Atmospheric Chemistry Experiment-Fourier Transform Spectrometer (ACE-FTS) indicates MIPAS-E PAN is higher than ACE-FTS in the UTLS by 70 ppt at the altitudes between 9.5–17.5 km, which lies within limits of

Title Page

Abstract

Introduction

Conclusions

References

Tables

Figures



Back

Close

Full Screen / Esc

Printer-friendly Version

Interactive Discussion



measurement error (Tereszchuk et al., 2013). This indicates that model simulated PAN concentrations in the UTLS show reasonable agreement with MIPAS-E.

The observed high concentrations during the monsoon season may be due to transport from the lower troposphere due to strong convection. Thus in order to study the influence of ASM circulation on the distribution of PAN in the UTLS region, the seasonal mean PAN concentrations (June–September) is analyzed. We present here estimates of the PAN climatology from MIPAS-E for the ASM season. Figure 2c and d exhibit the seasonal mean distributions PAN as observed by MIPAS at 14 km and 16 km respectively. PAN distribution obtained from ECHAM5-HAMMOZ reference simulations at 14 and 16 km are plotted in Fig. 2e and f respectively for comparison. Figure 2c and d show maxima in PAN concentrations (~ 200 – 250 ppt) over Asian monsoon anticyclone region (12 – 40° N, 20 – 120° E). The model is able to reproduce the maximum in PAN in the monsoon anticyclone, but simulated PAN concentrations are less than MIPAS observations.

To illustrate vertical transport in the Asian monsoon region, longitude-altitude cross-section averaged over monsoon anticyclone region 10 – 40° N and for June–September as obtained from MIPAS PAN observations and ECHAM5-HAMMOZ baseline simulations (8 – 23 km) are shown in Fig. 3a and b respectively. Both MIPAS observations and ECHAM5-HAMMOZ simulations show elevated levels of PAN (200 – 250 ppt) over the Bay of Bengal (near 80 – 100° E). The vertical winds plotted in Fig. 3b show cross tropopause transport from this region. Figure 3c reveals transport of boundary layer PAN to UTLS mainly from strong convection region extending from Bay of Bengal to South China Sea (~ 100 – 120° E) and Southern Flank of Himalaya (~ 80 – 90° E). In agreement with our results, previous studies also indicate significant vertical transport due to strong monsoon convection from the southern slopes of the Himalayas (Fu et al., 2006; Fadnavis et al., 2013) and the region spanned by the Bay of Bengal and the South China Sea (Park et al., 2009). The climatology of the Advanced Very High Resolution Radiometer (AVHRR), Atmospheric Infrared Sounder (AIRS), and Moderate Resolution Imaging Spectroradiometer (MODIS) observations show frequent deep

Regional impacts

S. Fadnavis et al.

Title Page

Abstract

Introduction

Conclusions

References

Tables

Figures

◀

▶

◀

▶

Back

Close

Full Screen / Esc

Printer-friendly Version

Interactive Discussion



Regional impacts

S. Fadnavis et al.

Title Page

Abstract

Introduction

Conclusions

References

Tables

Figures



Back

Close

Full Screen / Esc

Printer-friendly Version

Interactive Discussion



convection over the Bay of Bengal and over the foot hills of the Himalayas (Devasthale and Fueglistaler, 2010). From Trajectory analysis Chen et al. (2012) reported that the three dominant regions contributing to transport from the boundary layer to the tropical tropopause are: (i) the region between tropical Western Pacific region and South China Seas (38 %), (ii) the Bay of Bengal and South Asian subcontinent (BOB, 21 %), and (iii) the Tibetan Plateau including the South Slope of the Himalayas (12 %).

The latitude-altitude cross section of MIPAS-E PAN concentrations (averaged over 60–120° E) shows high levels of PAN over the northern subtropics (20–40° N) (see Fig. 3d). The model simulated PAN shows a similar distribution (see Fig. 3e). The simulated PAN distribution at the surface reveals that the observed high levels of PAN in the UTLS are from the subtropical boundary layer (see Fig. 3f) and are then transported upwards in deep convection. The PAN is also transported from 40–60° N reaching up to 16 km. This plume is related to the biomass burning activity during this season over North-east China, Siberia, Mongolia (figures not shown). The biomass-burning emissions estimated from satellites show intense biomass burning activity over these regions during monsoons season (Choi et al., 2013). In agreement with our results, ACE-FTS PAN measurements also shows plume (concentrations > 280 pptv) rising from Siberia (Tereszchuk et al., 2013).

The boundary layer PAN transport by deep convection may increase NO_x and hence change the ozone concentrations in the UTLS and at remote locations to where it gets transported by the Brewer Dobson circulation (Randel et al., 2010). Another model simulation study indicates that PAN increases ozone production by removing NO_x from regions of low ozone production efficiency and inject it into regions with higher ozone production efficiency, resulting in a global increase in ozone production by 2 % (Walker et al., 2010). The strong lightning activity during the monsoon season (Ranalkar and. Chaudhari, 2009; Penki and Kamra, 2013) enhances the concentrations of PAN species through production of NO_x (Tie et al., 2001, 2002; Labrador et al., 2005; Zhao et al., 2009; Cooper et al., 2009) that is released into a background atmosphere with some traces of VOCs. MOZART model simulations show that lightning

enhances PAN emissions $\sim 20\text{--}30\%$ and $\text{HNO}_3 \sim 60\text{--}80\%$ in the middle troposphere (Tie et al., 2001). ECHAM5-HAMMOZ simulations show lightning increase in NO_x of $\sim 50\text{--}70\%$, $\text{O}_3 \sim 20\text{--}35\%$, $\text{HNO}_3 \sim 50\text{--}75\%$ and PAN $\sim 20\text{--}35$ over the ASM, respectively (Fadnavis et al., 2014).

4 Trends in PAN in the UTLS of ASM region

Trends in PAN have been computed from MIPAS-E observation in the UTLS (8–23 km), over the ASM region (10–40° N, 60–120° E), India (8–35° N, 70–94° E) and China (20–45° N, 85–130° E). The trends are estimated with the method presented by von Clarmann et al. (2010). To estimate vertical profiles of annual and seasonal trends we took into account altitude dependent fit parameters: (1) a possible bias between the PAN values of the 2002–2004 and 2005–2011 measurement periods (details are documented by von Clarmann et al., 2010). (2) Amplitude and phase of the QBO, and (3) amplitudes and phases of periodic variations with periods of 3, 4, 6 and 12 months. The estimated trends are not significant at the altitudes between 8 km and 9 km due to the small number of data points. The trends from model simulations are calculated from difference between Ind38Chin73 and reference simulations. The estimated annual and seasonal trends are shown in Fig. 4a and b respectively. Model simulated and MIPAS-E observed PAN in the UTLS shows positive trends. The trends obtained from MIPAS-E observations are statistically significant at 2 Sigma level (except at few altitudes). The annual trends in MIPAS-E PAN vary between 0.1 ± 0.05 to 2.7 ± 0.8 ppt year⁻¹ over the ASM region, $0.4 \pm 1.3\text{--}3.2 \pm 0.49$ ppt year⁻¹ over India and $1.1 \pm 0.25\text{--}3.4 \pm 1.3$ ppt year⁻¹ over China. Trends over India are insignificant between 12–14 km. Figure 4a shows that in the upper troposphere (10–14 km) trends are higher over China as compared to India. In general the trend values are higher near the tropopause ($\sim 18\text{--}19$ km). The trends computed from model simulations are less than the trends obtained from MIPAS-E observations. However, they show similar regional variations. The model estimated trends over the ASM region vary between $0.1\text{--}1.9$ ppt year⁻¹, India $\sim 0.2\text{--}2.2$ ppt year⁻¹ and

Title Page

Abstract

Introduction

Conclusions

References

Tables

Figures



Back

Close

Full Screen / Esc

Printer-friendly Version

Interactive Discussion



Regional impacts

S. Fadnavis et al.

Title Page

Abstract

Introduction

Conclusions

References

Tables

Figures

◀

▶

◀

▶

Back

Close

Full Screen / Esc

Printer-friendly Version

Interactive Discussion



China $\sim 0.8\text{--}2.4\text{ ppt year}^{-1}$. The increases in transportation, industrialization, and the number of coal burning power plants results in the increase of NO_x over south and eastern Asia. The satellite observed positive trends of NO_x emissions over these regions (Ghude et al., 2013; Schneider and van der A, 2012) show coherence with estimated trends in MIPAS-E PAN. The estimated trends in MIPAS-E PAN during the monsoon season are larger than annual trends at the altitude above 16 km for all the three regions. At the altitudes below 14 km seasonal trends are less than annual trends.

During the monsoon season, the estimated trends are positive and statistically significant at 2 sigma level. Over India the seasonal trends in MIPAS-E PAN vary between 0.5 ± 0.8 and $2.7 \pm 0.47\text{ ppt year}^{-1}$. In the upper troposphere, observed trends are statistically insignificant and they are negative between 12–14 km. The trends are higher over the China than India varying between 0.95 ± 1.2 and $2.9 \pm 0.45\text{ ppt year}^{-1}$, indicating that Chinese emissions contribute more to the ASM anticyclone. The statistically insignificant positive and negative trends in the upper troposphere over India may be related to convective transport and removal of NO_x by wet scavenging in the region near southern part of Himalayas. Model simulations for enhanced NO_x emissions over India show a non-linear increase in PAN in the upper troposphere (see the discussions in Sect. 5.2). The variation of trends during the monsoon season computed from ECHAM5-HAMMOZ PAN is similar to the trends obtained from MIPAS-E PAN although the estimated trends are lower. They vary between $\sim 0.9\text{--}3\text{ ppt year}^{-1}$ over India, $\sim 1\text{--}4.5\text{ ppt year}^{-1}$ over China and $\sim 0.8\text{--}3.6\text{ ppt year}^{-1}$ over ASM. Trends are larger over China than India in the upper troposphere and vice-a versa in the lower stratosphere. Satellite observations also shows higher tropospheric NO_x concentrations over China compared to India (Schneider and van der A, 2012; Ghude et al., 2013). Because of higher absolute NO_x concentrations over China, the same percent change in emissions will lead to a larger PAN trend in this region compared to India. The amount of PAN observed in the anticyclone over the ASM region depends on the transport pathways of the air mass. During the monsoon season the air mass in the anticyclone is from Asia and East Asia where biomass burning activity is high. The PAN is formed

Regional impacts

S. Fadnavis et al.

Title Page

Abstract

Introduction

Conclusions

References

Tables

Figures



Back

Close

Full Screen / Esc

Printer-friendly Version

Interactive Discussion



rapidly in biomass burning smoke (Alvarado et al., 2010) hence air rich in biomass burning pollutants over these regions, transport high amount of PAN into the UTLS where temperatures are colder; hence it will retain more of PAN (Nowak et al., 2004).

The increasing trends in lightning activity during monsoon season (Penki and Kamra, 2013; Yang and Li, 2014) will increase lightning induced reactive nitrogen (NO_x), and nitrogen reservoir species (HNO_3 , PAN). The lightning-produced PAN is readily carried by convective updrafts to the lower stratosphere where its lifetime is considerably longer (Labrador et al., 2005). The increase in frequency of deep convective clouds over the tropical land mass (Aumann and Ruzmaikin, 2013) may cause increase in frequency of vertical transport. Radar, AVHRR, AIRS, and MODIS satellite observations show frequent overshoots deep into the tropical tropopause layer during monsoon season (Devasthale and Fueglistaler, 2010; Hassim et al., 2014). The vertical distribution of the seasonal trend suggests that there is increasing trend in transport of PAN into the lower stratosphere due to deep monsoon convection. Thus observed increases in UTLS PAN during the monsoon season is related to increase in trends in (1) emissions at the surface, (2) frequency of overshooting convection and (3) production from lightning.

In general, the trends estimated from MIPAS-E and ECHAM5-HAMMOZ PAN larger over China than India at altitudes below 14 km and vice-a versa above 14 km. This may be related with the amount of pollution outflow in the upper troposphere and lower stratosphere from India and China. The pollution from China released primarily below 14 km and Chinese emissions dominate over Indian emissions. The pollution from India has substantial outflow above 14 km due to convective lifting from southern slopes of Himalayas.

5 Impact of enhanced anthropogenic Asian NO_x on PAN, HNO_3 and O_3

The satellite observations and model simulations indicate that boundary layer pollutants are lofted into the UTLS by monsoon convection (Randel et al., 2010; Fadnavis et al., 2013, 2014). In the UTLS transport occurs through the monsoon anticyclone

and across the tropopause (Fadnavis et al., 2013). The transport of boundary layer Asian NO_x into the UTLS due to monsoon convection is evident in model simulations (see Fig. 5). In order to better understand the impact of enhanced anthropogenic Asian NO_x emission lifted to UTLS by ASM convection on the distribution of PAN, HNO_3 , and ozone we calculate percentage change of these constituents for the Ind38, Chin73, Ind38Chin38, Ind38Chin73 and Ind73 simulations with respect to reference simulations. Although we have analyzed horizontal (latitude-longitude) cross-sections at different altitudes within the UTLS (6–25 km), here we present plots only at 16 km as a representative of the tropical UTLS layer.

5.1 Impact on PAN

Figure 6a–e shows the percentage change in PAN at 16 km for Ind38, Chin73, Ind38Chin73, Ind38Chin38 and Ind73 simulations. The Ind38 simulation shows an increase in PAN of ~ 10 – 18 % with a 95 % significance level over China and the western Pacific Ocean between Indonesia and Japan. Similar high increases also occur over the northern Caspian Sea and over Weddell Sea near Antarctica. The increase in PAN is ~ 1 – 6 % over most of the other regions in middle and low latitudes. PAN decreases in polar regions reflecting a change in the diabatic circulation transport with enhanced descent of low PAN air at high latitudes in the stratosphere.

The Chin73 simulations show an increase in PAN of ~ 18 – 30 % over China, and western Pacific Ocean between Indonesia and Japan and 10 – 18 % over India. An increase in PAN of ~ 20 % is seen to the north of Japan and ~ 15 % over the Black Sea, southern Pacific Ocean, southern Indian Ocean and Australia. The increase in PAN over other subpolar regions is ~ 1 – 6 %. During the monsoon season, the westerly winds in the upper troposphere transport NO_x from China eastward over the Pacific Ocean. The increased values in the Southern Hemisphere middle latitudes similar to the maxima in the Northern Hemisphere middle latitudes indicate a change in the baroclinic eddy storm tracks. Since the PAN in the extratropics shown in Fig. 6 is in the lowermost stratosphere it is the change in the Rossby waves penetrating from the

tropospheric storm tracks that is producing the anomaly structure. These features are not simply due to extra PAN from increased emissions.

The Ind38Chin73 simulations (Fig. 6c) show increases of PAN $\sim 14\text{--}40\%$ over India, China and the western Pacific and $\sim 10\text{--}20\%$ over the Pacific Ocean ($30^\circ\text{N}\text{--}35^\circ\text{S}$).

This gives a combined picture of Ind38 and Chin73 simulations, indicating superposing of trends. The outflow over the Pacific Ocean is more pronounced compared to the Chin73 case as is to be expected given the Ind38 case shows transport over the western Pacific. The percentage increase of PAN in the Ind38Chin38 simulations (Fig. 6d) shows a $\sim 10\text{--}25\%$ increase over India, China, and the western Pacific Ocean as in the previous cases. The PAN increase pattern seen in the Ind38Chin38 case over central Asia and the Black Sea does not persist in the Ind38Chin73 case with non-uniform emissions increases. This highlights the nonlinearity of the middle latitude dynamical changes that are responsible for the PAN anomaly structure in the extratropics. The baroclinic eddy storm track changes are not the same for the two emissions scenarios. Nearer to the emissions source regions the PAN response is more linear.

Figure 6a–d indicates that increase in NO_x emissions over the Indian region lead to an increase of PAN over China and western Pacific Ocean while increase in NO_x emissions over China increases PAN over a larger region covering India, South East Asia and South China Sea, Indian Ocean and Pacific Ocean. An ensemble simulation for Ind73 emissions increased by 73 % instead of 38 % (Fig. 6e) produced much higher values of PAN in the anticyclone region but did not produce a significant increase in the outflow over the Pacific Ocean. The increase in PAN for Ind38Chin73 simulation is 5–20 % between 10–14 km and $\sim 20\text{--}40\%$ at the altitudes between 16–22 km over India and China. This is in agreement with observed trends in MIPAS-E PAN 0.5–2 % between 10–14 km and 2–4 % year^{-1} between 16–22 km. Comparison of Ind73 and Chin73 simulations show that PAN increases in the anticyclone are primarily due to Chinese emissions. Doubling (~ 1.9 times) the NO_x emissions over India increases the PAN amounts by $\sim 4\text{--}12\%$ over the ASM and western pacific in the UTLS. The nonlinear response to increases in NO_x emissions over India and China is related to

Regional impacts

S. Fadnavis et al.

Title Page

Abstract

Introduction

Conclusions

References

Tables

Figures

◀

▶

◀

▶

Back

Close

Full Screen / Esc

Printer-friendly Version

Interactive Discussion



Regional impacts

S. Fadnavis et al.

Title Page

Abstract

Introduction

Conclusions

References

Tables

Figures

◀

▶

◀

▶

Back

Close

Full Screen / Esc

Printer-friendly Version

Interactive Discussion



transport pathways. Emissions over India are transported in the monsoon anticyclone as the deep convection over the southern slopes of the Himalayas and Bay of Bengal injects emissions into the eastern core of the anticyclone. The anticyclone is an effective containment vessel for trace constituents in the UTLS around the tropopause level (Park et al., 2008). Park et al. (2009) found that emissions over India and the Bay of Bengal account for most of the CO in the anticyclone at 100 hPa and emissions over China make a secondary contribution (see their Figs. 9 and 10). Convective detrainment occurs primarily below 150 hPa, which is the case over China, and only part of it becomes entrained in the anticyclonic circulation with the rest being transported to the southwest in the Hadley circulation and the northeast over the Pacific Ocean (Jiang et al., 2007; Park et al., 2009). The PAN distribution in the lower troposphere (figures not included) for the Chin73 simulations, shows high amounts over the region from Bay of Bengal to South China Sea and the southern slopes of Himalayas. This is then transported to the UTLS by the monsoon convection since transport occurs from convective region covering Bay of Bengal to South China Sea and Southern slope of Himalaya (Fu et al., 2006; Park et al., 2009; Fadnavis et al., 2013). Thus increase in NO_x emissions over China shows increase in PAN over India, China and western pacific (Fig. 6b). This shows that emissions over China have a greater impact on PAN amounts in the UTLS. Some of this is due to differences in total emission amounts. But it appears that differences in the convective transport pathways, namely more significant transport over the Bay of Bengal and South China Seas, are playing a role.

5.2 Impact on HNO₃

Changes in distribution of HNO₃ (%) at 16 km due to enhanced anthropogenic Asian NO_x emissions are shown in Fig. 7a–e. Ind38 simulations show 1–5% increase in HNO₃ over most of the regions with a 95% statistically significant high of 10–14% over the South China Sea and a high of over 20–25% over the East China Sea. The Chin73 simulations show increase in HNO₃ in a region between 30° S and 30° N with few patches over other regions. There is a significant increase in HNO₃ ~ 14–40% over

Regional impacts

S. Fadnavis et al.

Title Page

Abstract

Introduction

Conclusions

References

Tables

Figures



Back

Close

Full Screen / Esc

Printer-friendly Version

Interactive Discussion



the monsoon anticyclone and over 30 % over South East Asia, China, South and East China Seas and over the western Pacific Ocean south of Japan. There is an increase (95 % confidence level) in HNO_3 of $\sim 8\text{--}14\%$ over the tropical Pacific Ocean extending to South America. The Ind38Chin73 and Ind38Chin38 simulations show statistically significant increases of HNO_3 in the monsoon anticyclone region. However, comparing the India and China uniform and non-uniform emissions increase cases it is apparent that a 38 % increase in NO_x emissions over China is not sufficient to drive a significant HNO_3 response over the central and eastern Pacific Ocean. The dynamical response to the NO_x emissions changes is such that HNO_3 is lower in most of the extratropics at 16 km. As noted above, this response is likely due to an intensification of the Brewer–Dobson circulation.

Figures 6 and 7 show that increase in NO_x emissions over India, increases PAN and HNO_3 in the UTLS over South East Asia and South China Sea. Concentration of these species is less over the Indian region especially near southern parts of Himalaya, from where boundary layer Indian pollutants are transported into the monsoon anticyclone (Fadnavis et al., 2013). However, increase in NO_x emissions over China increases PAN and HNO_3 into the monsoon anticyclone. Part of these emissions is taken up by the westerly winds and is transported over the Pacific Ocean. Similar increase in PAN and HNO_3 is also observed for Ind38Chin38 and Ind38Chin73 simulations. This indicates that emissions over China are fed more efficiently into the monsoon anticyclone than those over India. The low concentration of HNO_3 and PAN over the convection region of Himalaya may be due to removal of NO_x by wet scavenging. The latitude-longitude cross-section of ozone at 860 hPa show (figure not shown) for Ind38 simulations show high anomalies over India and making its way over the Pacific Ocean to North America. The longitudinal transect of HNO_3 (see Fig. 7f) indicates that HNO_3 is depleted around 100° East and this removal process is less effective going farther to the east, i.e. over China and South-East Asia. It is possible that the extra NO_x over India is being locked up as HNO_3 and removed by wet scavenging. High amount of water vapour present in the atmosphere during the monsoon season, may remove NO_x by the reactions:

Regional impacts

S. Fadnavis et al.

Title Page

Abstract

Introduction

Conclusions

References

Tables

Figures

◀

▶

◀

▶

Back

Close

Full Screen / Esc

Printer-friendly Version

Interactive Discussion



$\text{NO}_2 + \text{OH} \rightarrow \text{HNO}_3$ and $\text{N}_2\text{O}_5 + 2\text{H}_2\text{O} \rightarrow 2\text{HNO}_3$ that yields HNO_3 is more active in the convective zone south of the Himalayas. So the efficiency of NO_x conversion to HNO_3 is larger compared to that over China. A number of previous studies (Holland and Lamarque, 1997; Shepon et al., 2007) have reported that wet deposition of HNO_3 is the most important pathway of NO_x removal in the free troposphere. The ECHAM5-HAMMOZ analysis of convective heating and vertical ascent in the troposphere indicates that the transport pathway over the Bay of Bengal and the South China Sea is more active. These results are in agreement with Park et al. (2009), Fadnavis et al. (2013). This indicates that HNO_3 differences are not due to transport but may be by wet deposition.

5.3 Impact on Ozone

Changes in ozone at 16 km due to enhanced Asian anthropogenic NO_x are shown in Fig. 8a–e. Increase in NO_x emissions over India (Ind38), increases ozone (3–7 %) over the India Ocean and South China Sea. Chin38, Ind38Chin38, Ind38Chin73 simulations show increase in ozone (3–10 %) over India, Indian Ocean, South East Asia, South China Sea and Pacific Ocean, indicating transport along westerly winds. Increase in ozone over the Southern Indian Ocean may be due to transport of NO_x by brewer Dobson circulation. The uniform increase in NO_x over India and China (Ind73 and Chin73) simulations show more increase in ozone in the monsoon anticyclone from Chinese emissions than India. This is due to removal of NO_x by wet scavenging in the region near Himalayas. In the stratosphere, the impact of enhanced anthropogenic NO_x emissions is to reduce ozone. ECHAM5-HAMMOZ simulations show a reduction in ozone in the stratosphere (< 70 hPa). The highest ozone loss for the Ind38 simulation is ~ 0.5–2 % in the stratosphere.

6 Conclusions

Analysis of PAN estimates from MIPAS satellite for the period 2002–2011 and ECHAM5-HAMMOZ global model simulations shows transport of boundary layer PAN into the monsoon anticyclone due to strong convection. The latitude-altitude, longitude-altitude cross-section maps reveals transport mainly occur from strong convections region extending from Bay of Bengal to South China Sea ($\sim 100\text{--}120^\circ$ E) and the southern flank of Himalaya ($\sim 80\text{--}90^\circ$ E). These results are in agreement previous studies (Fu et al., 2006; Park et al., 2009; Fadnavis et al., 2013; Chen et al., 2012) indicating significant vertical transport by deep convection and diabatic heating induced upwelling. Although the model simulations reproduce the main features, e.g. maximum in monsoon anticyclone and vertical transport into the UTLS, the MIPAS-E PAN is higher than model by $\sim 30\text{--}60$ ppt. The comparison of MIPAS-E PAN measurements with ACE-FTS indicates that MIPAS-E PAN is higher by ~ 70 ppt at the altitudes between 9.5–17.5 km (Tereszczuk et al., 2013).

The MIPAS-E PAN observations in the UTLS over India and China show annual trends in PAN varying between 0.4 ± 1.3 and 3.2 ± 0.49 ppt year⁻¹ over India and 1 ± 0.25 and 3.4 ± 1.3 ppt year⁻¹ over China. The seasonal trends are positive varying between 0.5 ± 0.8 and 2.7 ± 0.47 ppt year⁻¹ over India and 0.95 ± 1.2 and 2.9 ± 0.45 ppt year⁻¹ over China. In general, the estimated trends are statistically significant at 2 sigma level except in the upper troposphere over India, where positive and negative trends are statistically insignificant. These statistically insignificant trends may be related to convective transport from the southern parts of Himalaya and removal of NO_x by wet scavenging. Model simulations for enhanced NO_x emissions over India also show a non-linear increase in PAN in the upper troposphere. The estimated seasonal trends are higher than annual trends at the altitude above 14 km over Indian, Chinese and ASM regions. This may be due to transport by stronger deep convective activity during the monsoon season as observed in radar, AVHRR, AIRS and MODIS (e.g. Devasthale and Fueglistaler, 2010; Hassim et al., 2014). The observed increasing frequency of over

Regional impacts

S. Fadnavis et al.

[Title Page](#)[Abstract](#)[Introduction](#)[Conclusions](#)[References](#)[Tables](#)[Figures](#)[Back](#)[Close](#)[Full Screen / Esc](#)[Printer-friendly Version](#)[Interactive Discussion](#)

Regional impacts

S. Fadnavis et al.

Title Page

Abstract

Introduction

Conclusions

References

Tables

Figures

◀

▶

◀

▶

Back

Close

Full Screen / Esc

Printer-friendly Version

Interactive Discussion



shooting convection over the tropical land mass (Aumann and Ruzmaikin, 2013) indicate increasing trend in transport across the tropical tropopause in agreement with our results. The trends estimated from observations and model simulations are higher over China as compared to India, at the altitude below 14 km and vice-a versa above 14 km.

This may be related with the amount of pollution outflow in the upper troposphere and lower stratosphere from India and China. The pollution from China is released primarily below 14 km and Chinese emissions dominate over Indian emissions. The pollution from India has substantial outflow above 14 km due to convective lifting from southern slopes of Himalayas.

The trends estimated from sensitivity simulations for Ind38Chin73 are less than the trends in MIPAS-E PAN. However it could reproduce variations similar to MIPAS-E observations, higher trends values over the china (compared to India) in the upper troposphere and vice-a versa in the lower stratosphere. The sensitivity simulations for increase in NO_x emissions over the Indian region lead to an increase of PAN, HNO_3 and ozone over China and western Pacific Ocean while increase in NO_x emissions over China increases PAN over larger region covering India, South East Asia and South China Sea, Indian Ocean and Pacific Ocean. Comparison of uniform increase in NO_x over India and China (Ind73 and Chin73) shows that the effects on PAN, HNO_3 and O_3 mixing ratios in the anticyclone are more pronounced for Chinese emissions than for Indian emissions. Doubling (~ 1.9 times) the NO_x emissions over India shows a non-linear increase in PAN, HNO_3 and O_3 over the ASM and western pacific UTLS. The non linear response is related to transport pathways. Emissions over India are injected at the eastern end of monsoon anticyclone by the deep convection over the southern slopes of the Himalayas and Bay of Bengal. Comparison of India and China simulations shows increase in NO_x over India result in less concentrations of PAN, HNO_3 over the Indian region especially near southern parts of Himalaya, from where boundary layer Indian pollutants are transported into the monsoon anticyclone. The low concentration of PAN and HNO_3 over this region is due to removal of NO_x by wet scavenging. This may be due to higher efficiency of NO_x conversion to HNO_3 over India compared to

Regional impacts

S. Fadnavis et al.

Title Page

Abstract

Introduction

Conclusions

References

Tables

Figures



Back

Close

Full Screen / Esc

Printer-friendly Version

Interactive Discussion



China. However, increase in NO_x emissions over China increases PAN and HNO_3 in the monsoon anticyclone. Part of these emissions is taken up by the westerly winds and is transported over the Pacific Ocean and as far as Atlantic. There is also westward transport by tropical easterlies which may explain part of the signal over the Atlantic Ocean in the tropics and the Southern Hemisphere. Cross-equatorial transport into the Southern Hemisphere over the south Indian Ocean occurs as well due to mixing by breaking Rossby waves around the equatorial tropopause and via the meridional overturning, or diabatic, circulation. This indicates that Chinese emissions have a greater impact on the concentrations of these species than Indian emissions.

Acknowledgements. The authors thank the High Power Computing Centre (HPC) in IITM, Pune, India, for providing computer resources. S. Fadnavis acknowledges with gratitude B. N. Goswami, Director of IITM, for his encouragement during the course of this study.

References

- Alvarado, M. J., Logan, J. A., Mao, J., Apel, E., Riemer, D., Blake, D., Cohen, R. C., Min, K.-E., Perring, A. E., Browne, E. C., Wooldridge, P. J., Diskin, G. S., Sachse, G. W., Fuelberg, H., Sessions, W. R., Harrigan, D. L., Huey, G., Liao, J., Case-Hanks, A., Jimenez, J. L., Cubison, M. J., Vay, S. A., Weinheimer, A. J., Knapp, D. J., Montzka, D. D., Flocke, F. M., Pollock, I. B., Wennberg, P. O., Kurten, A., Crounse, J., Clair, J. M. St., Wisthaler, A., Mikoviny, T., Yantosca, R. M., Carouge, C. C., and Le Sager, P.: Nitrogen oxides and PAN in plumes from boreal fires during ARCTAS-B and their impact on ozone: an integrated analysis of aircraft and satellite observations, *Atmos. Chem. Phys.*, 10, 9739–9760, doi:10.5194/acp-10-9739-2010, 2010.
- Anderson, J. G., Wilmoth, D. M., Smith, J. B., and Sayres, D. S.: UV dosage levels in summer: increased risk of ozone loss from convectively injected water vapor, *Science*, 337, 835–839, 2012.
- Aumann, H. H. and Ruzmaikin, A.: Frequency of deep convective clouds in the tropical zone from 10 years of AIRS data, *Atmos. Chem. Phys.*, 13, 10795–10806, doi:10.5194/acp-13-10795-2013, 2013.

Regional impacts

S. Fadnavis et al.

Title Page

Abstract

Introduction

Conclusions

References

Tables

Figures



Back

Close

Full Screen / Esc

Printer-friendly Version

Interactive Discussion



- Bhatt, B. C., Koh, T.-Y., Yamamoto, M., and Nakamura, K.: The diurnal cycle of convective activity over South Asia as diagnosed from METEOSAT-5 and TRMM data, *Terr. Atmos. Ocean. Sci.*, 21, 841–854, doi:10.3319/TAO.2010.02.04.01(A), 2010.
- Chen, B., Xu, X. D., Yang, S., and Zhao, T. L.: Climatological perspectives of air transport from atmospheric boundary layer to tropopause layer over Asian monsoon regions during boreal summer inferred from Lagrangian approach, *Atmos. Chem. Phys.*, 12, 5827–5839, doi:10.5194/acp-12-5827-2012, 2012.
- Choi Ki-Chul, Woo, J.-H., Kim, H. K., Choi, J., Eum, J.-H., and Baek, B. H.: Modeling of Emissions from Open Biomass Burning in Asia Using the BlueSky Framework, *Asian Journal of Atmospheric Environment*, 7-1, 25–37, doi:10.5572/ajae.2013.7.1.025, 2013.
- Cooper, O. R., Eckhardt, S., Crawford, J. H., Brown, C. C., Cohen, R. C., Bertram, T. H., Wooldridge, P., Perring, A., Brune, W. H., Ren, X., Brunner, D., and Baughcum, S. L.: Summertime buildup and decay of lightning NO_x and aged thunderstorm outflow above North America, *J. Geophys. Res.*, 114, D01101, doi:10.1029/2008JD010293, 2009.
- Devasthale, A. and Fueglistaler, S.: A climatological perspective of deep convection penetrating the TTL during the Indian summer monsoon from the AVHRR and MODIS instruments, *Atmos. Chem. Phys.*, 10, 4573–4582, doi:10.5194/acp-10-4573-2010, 2010.
- Dodion, J., Fussen, D., Vanhellefont, F., Bingen, C., Mateshvili, N., Gilbert, K., Skelton, R., Turnball, D., McLeod, S. D., Boone, C. D., Walker, K. A., and Bernath, P. F.: Aerosols and clouds in the upper troposphere-lower stratosphere region detected by GOMOS and ACE: intercomparison and analysis of the years 2004 and 2005, *Adv. Space Res.*, 42, 1730–1742, doi:10.1016/j.asr.2007.09.027, 2008.
- Emmons, L. K., Hauglustaine, D. A., Muller, J.-F., Carroll, M. A., Brasseur, G. P., Brunner, D., Staehelin, J., Thouret, V., and Marenco, A.: Data composites of tropospheric ozone and its precursors from aircraft measurements, *J. Geophys. Res.*, 105, 20497–20538, 2000.
- Fadnavis, S., Semeniuk, K., Pozzoli, L., Schultz, M. G., Ghude, S. D., Das, S., and Kakatkar, R.: Transport of aerosols into the UTLS and their impact on the Asian monsoon region as seen in a global model simulation, *Atmos. Chem. Phys.*, 13, 8771–8786, doi:10.5194/acp-13-8771-2013, 2013.
- Fadnavis, S., Semeniuk, K., Martin, G. Schultz, M. G., Mahajan, A. S., Luca Pozzoli, L., Sonbawane, S., and Kiefer, M.: Transport pathways of peroxyacetyl nitrate in the upper troposphere and lower stratosphere from different monsoon systems during the summer monsoon Season, *Atmos. Chem. Phys. Discuss.*, in press, 2014.

Regional impacts

S. Fadnavis et al.

Title Page

Abstract

Introduction

Conclusions

References

Tables

Figures

◀

▶

◀

▶

Back

Close

Full Screen / Esc

Printer-friendly Version

Interactive Discussion



- Fiore, A. M., Horowitz, L. W., Purves, D. W., Levy II, H., Evans, M. J., Wang, Y., Li, Q., and Yantosca, R. M.: Evaluating the contribution of changes in isoprene emissions to surface ozone trends over the eastern United States, *J. Geophys. Res.*, 110, D12303, doi:10.1029/2004JD005485, 2005.
- 5 Fischer, E. V., Jacob, D. J., Yantosca, R. M., Sulprizio, M. P., Millet, D. B., Mao, J., Paulot, F., Singh, H. B., Roiger, A., Ries, L., Talbot, R.W., Dzepina, K., and Pandey Deolal, S.: Atmospheric peroxyacetyl nitrate (PAN): a global budget and source attribution, *Atmos. Chem. Phys.*, 14, 2679–2698, doi:10.5194/acp-14-2679-2014, 2014.
- Fischer, H. and Oelhaf, H.: Remote sensing of vertical profiles of atmospheric trace constituents with MIPAS limb-emission spectrometers, *Appl. Optics*, 35, 2787–2796, 1996.
- 10 Fischer, H., Birk, M., Blom, C., Carli, B., Carlotti, M., von Clarmann, T., Delbouille, L., Dudhia, A., Ehnhalt, D., Endemann, M., Flaud, J. M., Gessner, R., Kleinert, A., Koopman, R., Langen, J., López-Puertas, M., Mosner, P., Nett, H., Oelhaf, H., Perron, G., Remedios, J., Ridolfi, M., Stiller, G., and Zander, R.: MIPAS: an instrument for atmospheric and climate research, *Atmos. Chem. Phys.*, 8, 2151–2188, doi:10.5194/acp-8-2151-2008, 2008.
- 15 Fu, R., Hu, Y., Wright, J. S., Jiang, J. H., Dickinson, R. E., Chen, M., Filipiak, M., Read, W. G., Waters, J. W., and Wu, D. L.: Short circuit of water vapour and polluted air to the global stratosphere by convective transport over the Tibetan Plateau, *P. Natl. Acad. Sci. USA*, 103, 5664–5669, 2006.
- 20 Ganzeveld, L. and Lelieveld, J.: Dry deposition parameterization in a chemistry general circulation model and its influence on the distribution of reactive trace gases, *J. Geophys. Res.*, 100, 20999–21012, doi:10.1029/95JD02266, 1995.
- Gettelman, A., Kinnison, D. E., Dunkerton, T. J., and Brasseur, G. P.: The impact of monsoon circulations on the upper troposphere and lower stratosphere, *J. Geophys. Res.*, 109, D22101, doi:10.1029/2004JD004878, 2004.
- 25 Ghude, S. D., Kulkarni, S. H., Jena, C., Pfister, G. G., Beig, G., Fadnavis, S., and van der A, R. J.: Application of satellite observations for identifying regions of dominant sources of nitrogen oxides over the Indian Subcontinent, *J. Geophys. Res.*, 118, 1–15, doi:10.1029/2012JD017811, 2013.
- 30 Glatthor, N., von Clarmann, T., Fischer, H., Funke, B., Grabowski, U., Höpfner, M., Kellmann, S., Kiefer, M., Linden, A., Milz, M., Steck, T., and Stiller, G. P.: Global peroxyacetyl nitrate (PAN) retrieval in the upper troposphere from limb emission spectra of the Michelson Interfer-

Regional impacts

S. Fadnavis et al.

Title Page

Abstract

Introduction

Conclusions

References

Tables

Figures



Back

Close

Full Screen / Esc

Printer-friendly Version

Interactive Discussion



ometer for Passive Atmospheric Sounding (MIPAS), *Atmos. Chem. Phys.*, 7, 2775–2787, doi:10.5194/acp-7-2775-2007, 2007.

Hassim, M. E. E., Lane, T. P., and May, P. T.: Ground-based observations of overshooting convection during the Tropical Warm Pool-International Cloud Experiment, *J. Geophys. Res.-Atmos.*, 119, 880–905, doi:10.1002/2013JD020673, 2014.

Hilboll, A., Richter, A., and Burrows, J. P.: Long-term changes of tropospheric NO₂ over megacities derived from multiple satellite instruments, *Atmos. Chem. Phys.*, 13, 4145–4169, doi:10.5194/acp-13-4145-2013, 2013.

Holland, E. A. and Lamarque, J. F.: Modeling bio-atmospheric coupling of the nitrogen cycle through NO_x emissions and NO_y deposition, *Nutr. Cycl. Agroecosyst.*, 48, 7–24, 1997.

Horowitz, L. W., Walters, S., Mauzerall, D. L., Emmons, L. K., Rasch, P. J., Granier, C., Tie, X., Lamarque, J., Schultz, M. G., Tyndall, G. S., Orlando, J. J., and Brasseur, G. P.: A global simulation of tropospheric ozone and related tracers, Description and evaluation of MOZART, version 2, *J. Geophys. Res.*, 108, 4784, doi:10.1029/2002JD002853, 2003.

Jiang, J. H., Livesey, N. J., Su, H., Neary, L., McConnell, J. C., and Richards, N. A. D.: Connecting surface emissions, convective uplifting, and long-range transport of carbon monoxide in the upper troposphere: new observations from the Aura Microwave Limb Sounder, *Geophys. Res. Lett.*, 34, L18812, doi:10.1029/2007GL030638, 2007.

Keim, C., Liu, G. Y., Blom, C. E., Fischer, H., Gulde, T., Höpfner, M., Piesch, C., Ravegnani, F., Roiger, A., Schlager, H., and Sitnikov, N.: Vertical profile of peroxyacetyl nitrate (PAN) from MIPAS-STR measurements over Brazil in February 2005 and its contribution to tropical UT NO_y partitioning, *Atmos. Chem. Phys.*, 8, 4891–4902, doi:10.5194/acp-8-4891-2008, 2008.

Labrador, L. J., von Kuhlmann, R., and Lawrence, M. G.: The effects of lightning-produced NO_x and its vertical distribution on atmospheric chemistry: sensitivity simulations with MATCH-MPIC, *Atmos. Chem. Phys.*, 5, 1815–1834, doi:10.5194/acp-5-1815-2005, 2005.

Li, Q., Jiang, J. H., Wu, D. L., Read, W. G., Livesey, N. J., Waters, J. W., Zhang, Y., Wang, B., Filipiak, M. J., Davis, C. P., Turquety, S., Wu, S., Park, R. J., Yantosca, R. M., and Jacob, D. J.: Convective outflow of South Asian pollution: a global CTM simulation compared with EOS MLS observations, *Geophys. Res. Lett.*, 32, L14826, doi:10.1029/2005GL022762, 2005.

Nesbitt, S. W., Zhang, R., and Orville, R. E.: Seasonal and global NO_x production by lightning estimated from the optical transient detector (OTD), *Tellus B*, 52, 1206–1215, 2000.

Nowak, J., Parris, D. D., Neuman, J. A., Holloway, J. S., Cooper, O. R., Ryerson, T. B., Nicks, D. K., Flocke, F., Roberts, J. M., Atlas, E., de Gouw, J. A., Donnelly, S., Dun-

Regional impacts

S. Fadnavis et al.

Title Page

Abstract

Introduction

Conclusions

References

Tables

Figures



Back

Close

Full Screen / Esc

Printer-friendly Version

Interactive Discussion



lea, E., Hubler, G., Huey, L. G., Schauffler, S., Tanner, D. J., Warneke, C., and Fehsenfeld, F. C. S.: Gas-phase chemical characteristics of Asian emission plumes observed during ITCT 2K2 over the eastern North Pacific Ocean, *J. Geophys. Res.*, 109, D23S19, doi:10.1029/2003JD004488, 2004.

5 Ohara, T., Akimoto, H., Kurokawa, J., Horii, N., Yamaji, K., Yan, X., and Hayasaka, T.: An Asian emission inventory of anthropogenic emission sources for the period 1980–2020, *Atmos. Chem. Phys.*, 7, 4419–4444, doi:10.5194/acp-7-4419-2007, 2007.

Park, M., Randel, W. J., Kinnison, D. E., Garcia, R. R., and Choi, W.: Seasonal variation of methane, water vapour, and nitrogen oxides near the tropopause: satellite observations and model simulations, *J. Geophys. Res.*, 109, D03302, doi:10.1029/2003JD003706, 2004.

10 Park, M., Randel, W. J., Gettleman, A., Massie, S. T., and Jiang, J. H.: Transport above the Asian summer monsoon anticyclone inferred from Aura Microwave Limb Sounder tracers, *J. Geophys. Res.*, 112, D16309, doi:10.1029/2006JD008294, 2007.

15 Park, M., Randel, W. J., Emmons, L. K., Bernath, P. F., Walker, K. A., and Boone, C. D.: Chemical isolation in the Asian monsoon anticyclone observed in Atmospheric Chemistry Experiment (ACE-FTS) data, *Atmos. Chem. Phys.*, 8, 757–764, doi:10.5194/acp-8-757-2008, 2008.

Park, M., Randel, W. J., Emmons, L. K., and Livesey, N. J.: Transport pathways of carbon monoxide in the Asian summer monsoon diagnosed from Model of Ozone and Related Tracers (MOZART), *J. Geophys. Res.*, 114, D08303, doi:10.1029/2008JD010621, 2009.

20 Penki, R. K. and Kamra, A. K.: Lightning distribution with respect to the monsoon trough position during the Indian summer monsoon season, *J. Geophys. Res.*, 118, 4780–4787, doi:10.1002/jgrd.50382, 2013.

25 Pozzoli, L., Bey, I., Rast, J. S., Schultz, M. G., Stier, P., and Feichter, J.: Trace gas and aerosol interactions in the fully coupled model of aerosol-chemistry-climate ECHAM5- HAMMOZ: 1. Model description and insights from the spring 2001 TRACE-P experiment, *J. Geophys. Res.*, 113, D07308, doi:10.1029/2007JD009007, 2008a.

30 Pozzoli, L., Bey, I., Rast, J. S., Schultz, M. G., Stier, P., and Feichter, J.: Trace gas and aerosol interactions in the fully coupled model of aerosol-chemistry-climate ECHAM5-HAMMOZ: 2. Impact of heterogeneous chemistry on the global aerosol distributions, *J. Geophys. Res.*, 113, D07309, doi:10.1029/2007JD009008, 2008b.

Pozzoli, L., Janssens-Maenhout, G., Diehl, T., Bey, I., Schultz, M. G., Feichter, J., Vignati, E., and Dentener, F.: Re-analysis of tropospheric sulfate aerosol and ozone for the period 1980–

Regional impacts

S. Fadnavis et al.

Title Page

Abstract

Introduction

Conclusions

References

Tables

Figures



Back

Close

Full Screen / Esc

Printer-friendly Version

Interactive Discussion



- 2005 using the aerosol-chemistry-climate model ECHAM5-HAMMOZ, *Atmos. Chem. Phys.*, 11, 9563–9594, doi:10.5194/acp-11-9563-2011, 2011.
- Ranalkar, M. R. and Chaudhari, H. S.: Seasonal variation of lightning activity over the Indian subcontinent, *Meteorol. Atmos. Phys.*, 104, 125–134, 2009.
- 5 Randel, W. J. and Jensen, E. J.: Physical processes in the tropical tropopause layer and their roles in a changing climate, *Nat. Geosci.*, 6, 169–176, doi:10.1038/ngeo1733, 2013.
- Randel, W. J. and Park, M.: Deep convective influence on the Asian summer monsoon anticyclone and associated tracer variability observed with Atmospheric Infrared Sounder (AIRS), *J. Geophys. Res.*, 111, D12314, doi:10.1029/2005JD006490, 2006.
- 10 Randel, W. J., Park, M., Emmons, L., Kinnison, D., Bernath, P., Walker, K. A., Boone, C., and Pumphrey, H.: Asian monsoon transport of pollution to the stratosphere, *Science*, 30, 611–613, 2010.
- Ravishankara, A. R.: Water vapor in the lower stratosphere, *Science*, 337, 809–810, 6096, doi:10.1126/science.1227004, 2012.
- 15 Ridley, B. A., Madronich, S., Chatfield, R. B., Walega, J. G., Shetter, R. E., Carroll, M. A., and Montzka, D. D: Measurements and model simulations of the photostationary state during the Mauna Loa Observatory Photochemistry Experiment: implications for radical concentrations and ozone production and loss rates, *J. Geophys. Res.*, 97, 10375–10388, doi:10.1029/91JD02287, 1992.
- 20 Roeckner, E., Bauml, G., Bonaventura, L., Brokopf, R., Esch, M., Giorgetta, M., Hagemann, S., Kirchner, I., Kornblueh, L., Manzini, E., Rhodin, A., Schlese, U., Schulzweida, U., and Tompkins, A.: The atmospheric general circulation model ECHAM5: Part 1, Tech. Rep. 349, Max Planck Institute for Meteorology, Hamburg, 2003.
- Sander, S. P., Fried, R. R., Barker, J. R., Golden, D. M., Kurylo, M. J., Wine, P. H., J. Abbatt, P. D., Burkholder, J. B., Kolb, C. E., Moortgat, G. K., Huie, R. E., and Orkin, V. L.: Chemical kinetics and photochemical data for use in atmospheric studies, evaluation number 14, JPL Publ. 02-25, Jet Propul. Lab., Calif. Inst. of Technol., Pasadena, available at: http://jpldataeval.jpl.nasa.gov/pdf/JPL_02-25_rev02.pdf (last access: February 2003), 2003.
- 25 Sander, S. P., Finlayson-Pitts, B. J., Friedl, R. R., Golden, D. M., Huie, R. E., Keller-Rudek, H., Kolb, C. E., Kurylo, M. J., Molina, M. J., Moortgat, G. K., Orkin, V. L., Ravishankara, A. R., and Wine, P. H.: Chemical Kinetics and Photochemical Data for Use in Atmospheric Studies, Evaluation Number 15, JPL Publication 06-2, Jet Propulsion Laboratory, Pasadena, available at: <http://jpldataeval.jpl.nasa.gov> (last access: July 2006), 2006.
- 30

Regional impacts

S. Fadnavis et al.

Title Page

Abstract

Introduction

Conclusions

References

Tables

Figures



Back

Close

Full Screen / Esc

Printer-friendly Version

Interactive Discussion



Schneider, P. and van der A, R. J.: A global single-sensor analysis of 2002–2011 tropospheric nitrogen dioxide trends observed from space, *J. Geophys. Res.*, 117, D16309, doi:10.1029/2012JD017571, 2012.

Schultz, M. G., Jacob, D. J., Wang, Y., Logan, J. A., Atlas, E. L., Blake, D. R. J., Blake, N. J., Bradshaw, J. D., Browell, E. V., Fenn, M. A., Flocke, F., Gregory, G. L., Heikes, B. G., Sachse, G. W., Sandholm, S. T., Shetter, R. E., Singh, H. B., and Talbot, R. W.: On the origin of tropospheric ozone and NO_x over the tropical south Pacific, *J. Geophys. Res.*, 104, 5829–5843, 1999.

Shepon, A., Gildor, H., Labrador, L. J., Butler, T., Ganzeveld, L. N., and Lawrence, M. G.: Global reactive nitrogen deposition from lightning NO_x , *J. Geophys. Res.*, 112, D06304, doi:10.1029/2006JD007458, 2007.

Sillman, S. and Samson, P. J.: Impact of temperature on oxidant photochemistry in urban, polluted rural and remote environments, *J. Geophys. Res.*, 100, 11497–11508, doi:10.1029/94jd02146, 1995

Singh, H. B., and Hanst, P. L.: Peroxyacetyl nitrate (PAN) in the unpolluted atmosphere: an important reservoir for nitrogen oxides, *Geophys. Res. Lett.*, 8, 941–944, 1981.

Singh, H. B., Salas, L. J., and Viezee, W.: Global distribution of peroxyacetyl nitrate, *Nature*, 321, 588–591, 1986.

Singh, H. B., Viezee, W., Chen, Y., Thakur, A. N., Kondo, Y., and Talbot, R. W., Gregory, G. L., Sachse, G. W., Blake, D. R., Bradshaw, J. D., Wang, Y., and Jacob, D. J.: Latitudinal distribution of reactive nitrogen in the free troposphere over the Pacific Ocean in late winter/early spring, *J. Geophys. Res.*, 103, 28237–28246, doi:10.1029/98JD01891, 1998.

Sinha, V., Kumar, V., and Sarkar, C.: Chemical composition of pre-monsoon air in the Indo-Gangetic Plain measured using a new air quality facility and PTR-MS: high surface ozone and strong influence of biomass burning, *Atmos. Chem. Phys.*, 14, 5921–5941, doi:10.5194/acp-14-5921-2014, 2014.

Stier, P., Feichter, J., Kinne, S., Kloster, S., Vignati, E., Wilson, J., Ganzeveld, L., Tegen, I., Werner, M., Balkanski, Y., Schulz, M., Boucher, O., Minikin, A., and Petzold, A.: The aerosol-climate model ECHAM5-HAM, *Atmos. Chem. Phys.*, 5, 1125–1156, doi:10.5194/acp-5-1125-2005, 2005.

Tereszchuk, K. A., Moore, D. P., Harrison, J. J., Boone, C. D., Park, M., Remedios, J. J., Randel, W. J., and Bernath, P. F.: Observations of peroxyacetyl nitrate (PAN) in the upper tro-

Regional impacts

S. Fadnavis et al.

Title Page

Abstract

Introduction

Conclusions

References

Tables

Figures



Back

Close

Full Screen / Esc

Printer-friendly Version

Interactive Discussion



- posphere by the Atmospheric Chemistry Experiment-Fourier Transform Spectrometer (ACE-FTS), *Atmos. Chem. Phys.*, 13, 5601–5613, doi:10.5194/acp-13-5601-2013, 2013.
- Tie, X. X., Zhang, R., Brasseur, G., Emmons, L., and Lei, W.: Effects of lightning on reactive nitrogen and nitrogen reservoir species in the troposphere, *J. Geophys. Res.-Atmos.*, 106, 3167–3178, doi:10.1029/2000JD900565, 2001.
- Tie, X., Zhang, R., Brasseur, G., and Lei, W.: Global NO_x production by lightning, *J. Atmos. Chem.*, 43, 61–74, 2002.
- Vernier, J. P., Thomason, L. W., and Kar, J.: CALIPSO detection of an Asian tropopause aerosol layer, *Geophys. Res. Lett.*, 38, L07804, doi:10.1029/2010GL046614, 2011.
- von Clarmann, T., Höpfner, M., Kellmann, S., Linden, A., Chauhan, S., Funke, B., Grabowski, U., Glatthor, N., Kiefer, M., Schieferdecker, T., Stiller, G. P., and Versick, S.: Retrieval of temperature, H₂O, O₃, HNO₃, CH₄, N₂O, ClONO₂ and ClO from MIPAS reduced resolution nominal mode limb emission measurements, *Atmos. Meas. Tech.*, 2, 159–175, doi:10.5194/amt-2-159-2009, 2009.
- Walker, T. W., Martin, R. V., van Donkelaar, A., Leaitch, W. R., MacDonald, A. M., Anlauf, K. G., Cohen, R. C., Bertram, T. H., Huey, L. G., Avery, M. A., Weinheimer, A. J., Flocke, F. M., Tarasick, D. W., Thompson, A. M., Streets, D. G., and Liu, X.: Trans-Pacific transport of reactive nitrogen and ozone to Canada during spring, *Atmos. Chem. Phys.*, 10, 8353–8372, doi:10.5194/acp-10-8353-2010, 2010.
- Wiegele, A., Glatthor, N., Höpfner, M., Grabowski, U., Kellmann, S., Linden, A., Stiller, G., and von Clarmann, T.: Global distributions of C₂H₆, C₂H₂, HCN, and PAN retrieved from MIPAS reduced spectral resolution measurements, *Atmos. Meas. Tech.*, 5, 723–734, doi:10.5194/amt-5-723-2012, 2012.
- Wu, Z., Wang, X., Turnipseed, A. A., Chen, F., Zhang, L., Guenther, A. B., Karl, T., Huey, L. G., Niyogi, D., Xia, B., and Alapaty, K.: Evaluation and improvements of two community models in simulating dry deposition velocities for peroxyacetyl nitrate (PAN) over a coniferous forest, *J. Geophys. Res.*, 117, D04310, doi:10.1029/2011JD016751, 2012.
- Xiong, X., Houweling, S., Wei, J., Maddy, E., Sun, F., and Barnet, C.: Methane plume over south Asia during the monsoon season: satellite observation and model simulation, *Atmos. Chem. Phys.*, 9, 783–794, doi:10.5194/acp-9-783-2009, 2009.
- Yamaji, K., Ohara, T., Uno, I., Tanimoto, H., Kurokawa, J., Akimoto, H.: Analysis of the seasonal variation of ozone in the boundary layer in East Asia using the Community Multi-scale Air

Quality model: what controls surface ozone levels over Japan?, Atmos. Environ., 40, 1856–1868, 2006.

Yang, X. and Li, Z.: Increases in thunderstorm activity and relationships with air pollution in southeast China, J. Geophys. Res.-Atmos., 119, 1835–1844, doi:10.1002/2013JD021224, 2014.

Zhao, C., Wang, Y., Choi, Y., and Zeng, T.: Summertime impact of convective transport and lightning NO_x production over North America: modeling dependence on meteorological simulations, Atmos. Chem. Phys., 9, 4315–4327, doi:10.5194/acp-9-4315-2009, 2009.

Regional impacts

S. Fadnavis et al.

Title Page

Abstract

Introduction

Conclusions

References

Tables

Figures



Back

Close

Full Screen / Esc

Printer-friendly Version

Interactive Discussion



Table 1. Global aircraft measurements used for model evaluation.

Experiment	Date Frame	Species	Location
POLINAT-2 (Falcon)	19 Sep–Oct 25, 1997	O ₃ , NO _x	Canary-Islands: LAT = 25, 35 LON = 340, 350 E-Atlantic: LAT = 35, 45 LON = 330, 340 Europe: LAT = 45, 55 LON = 5, 15 Ireland: LAT = 50, 60 LON = 345, 355
PEM-Tropics-A (DC8)	24 Aug–15 Oct, 1996	O ₃ , NO _x , HNO ₃ , PAN	Christmas-Island: LAT = 0, 10 LON = 200, 220 Easter-Island: LAT = -40, -20 LON = 240, 260 Fiji: LAT = -30, -10 LON = 170, 190 Hawaii: LAT = 10, 30 LON = 190, 210 Tahiti: LAT = -20, 0 LON = 200, 230
PEM-Tropics-A (P3)	15 Aug–26 Sep, 1996	O ₃ , HNO ₃	Christmas-Island: LAT = 0, 10 LON = 200, 220 Easter-Island: LAT = -40, -20 LON = 240, 260 Hawaii: LAT = 10, 30 LON = 190, 210 Tahiti: LAT = -20, 0 LON = 200, 230
ABLE-3B (Electra)	6 Jul–15 Aug, 1990	O ₃ , NO _x , HNO ₃ , PAN	Labrador: LAT = 50, 55 LON = 300, 315 Ontario: LAT = 45, 60 LON = 270, 280 US-E-Coast: LAT = 35, 45 LON = 280, 290
CITE-3 (Electra)	22 Aug–29 Sep, 1989	O ₃ , NO _x	Natal: LAT = -15, 5 LON = 325, 335 Wallops: LAT = 30, 40 LON = 280, 290
ELCHEM (Sabreliner)	27 Jul–22 Aug, 1989	O ₃ , NO _x	New-Mexico: LAT = 30, 35 LON = 250, 255
ABLE-3A (Electra)	7 Jul–17 Aug, 1988	O ₃ , NO _x , PAN	Alaska: LAT = 55, 75 LON = 190, 205
ABLE-2A (Electra)	12 Jul–13 Aug, 1985	O ₃	E-Brazil: LAT = -10, 0 LON = 300, 315 W-Brazil: LAT = -5, 0 LON = 290, 300
STRATOZ-3 (Caravelle 116)	4–26 Jun, 1984	O ₃	Brazil: LAT = -20, 0 LON = 315, 335 Canary-Islands: LAT = 20, 35 LON = 340, 355 E-Tropical-N-Atlantic: LAT = 0, 20 LON = 330, 345 England: LAT = 45, 60 LON = -10, 5 Goose-Bay: LAT = 45, 60 LON = 290, 305 Greenland: LAT = 60, 70 LON = 290, 330 Iceland: LAT = 60, 70 LON = 330, 355 NW-South-America: LAT = -5, 10 LON = 275, 295 Puerto-Rico: LAT = 10, 25 LON = 290, 300 S-South-America: LAT = -65, -45 LON = 275, 300 SE-South-America: LAT = -45, -20 LON = 295, 320 SW-South-America: LAT = -45, -25 LON = 285, 292 Spain: LAT = 35, 45 LON = -15, 0 W-Africa: LAT = 0, 15 LON = -15, 0 W-South-America: LAT = -25, -5 LON = 275, 290 Western-N-Atlantic: LAT = 25, 45 LON = 290, 300
CITE-2 (Electra)	11 Aug–5 Sep, 1986	O ₃ , NO _x , HNO ₃ , PAN	Calif: LAT = 35, 45 LON = 235, 250 Pacific: LAT = 30, 45 LON = 225, 235

Title Page

Abstract

Introduction

Conclusions

References

Tables

Figures



Back

Close

Full Screen / Esc

Printer-friendly Version

Interactive Discussion



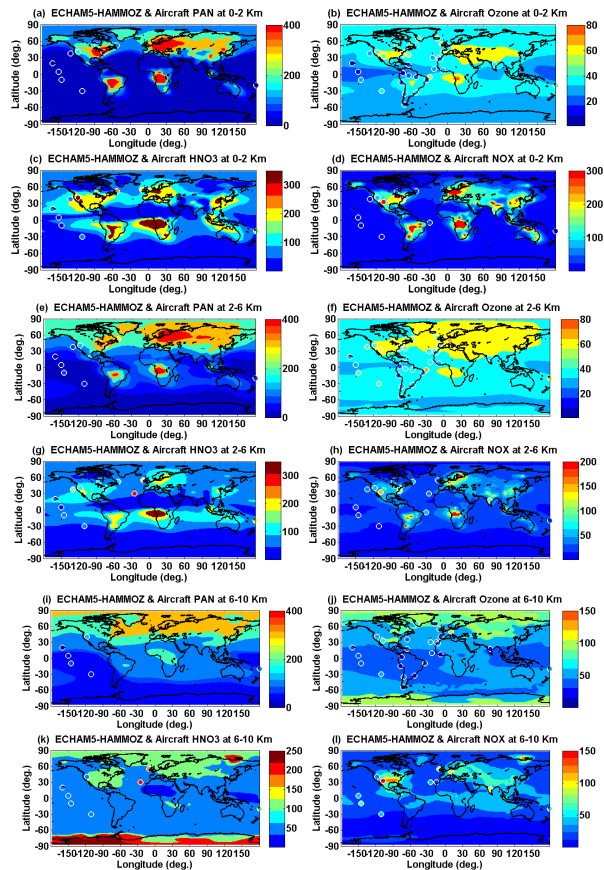


Figure 1. Global mean distribution of PAN (ppt), ozone (ppb), HNO_3 (ppt) and NO_x (ppt) averaged for the monsoon season and altitude ranges. Model results for 1995–2004 (background solid contours) are compared to observations from Table 1 for all years (filled circles). Aircraft observations are averaged vertically and horizontally over the flight region.

[Title Page](#)
[Abstract](#)
[Introduction](#)
[Conclusions](#)
[References](#)
[Tables](#)
[Figures](#)
[Back](#)
[Close](#)
[Full Screen / Esc](#)
[Printer-friendly Version](#)
[Interactive Discussion](#)

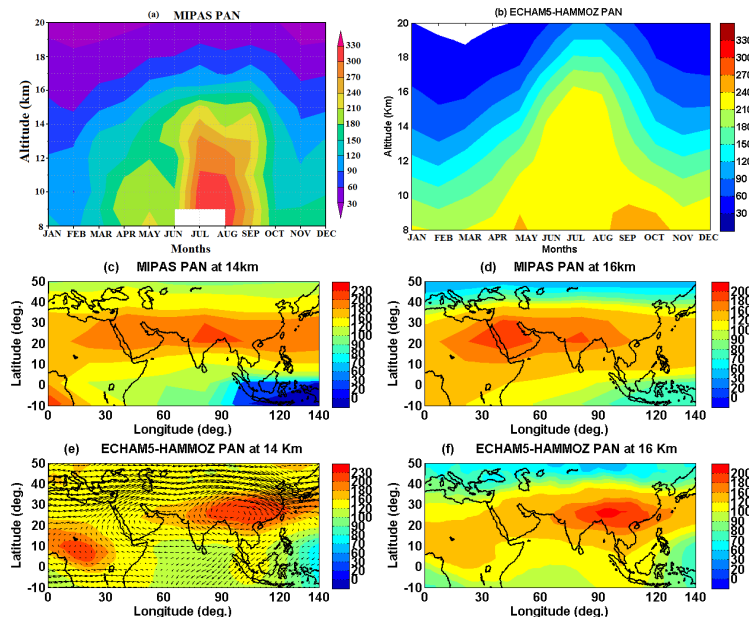



Figure 2. The seasonal cycle of PAN (ppt) averaged over anticyclone region (60–120° E, 10–40° N) **(a)** as observed by MIPAS and for the period 2002–2011 **(b)** ECHAM5-HAMMOZ reference simulation. Distribution of seasonal mean PAN concentration (ppt) as observed by MIPAS (climatology for the period 2002–2011) at **(c)** 14 km **(d)** 16 km and ECHAM5-HAMMOZ reference simulation at **(e)** 14 km **(f)** 16 km. ECHAM5-HAMMOZ simulations are smoothed with averaging kernel of MIPAS. Wind vectors are indicated by black arrows in **(e)**.

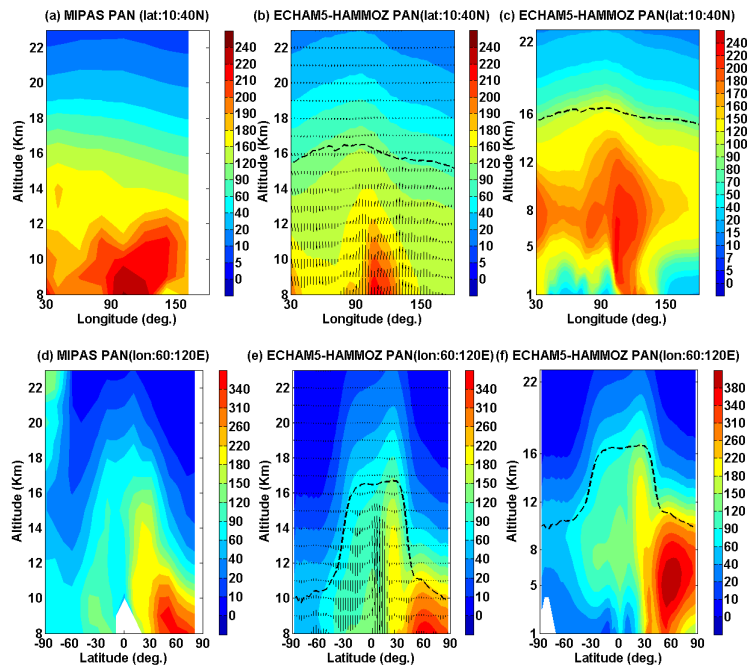


Figure 3. Longitude-altitude cross section of PAN (ppt) averaged for the monsoon season and 10–40° N **(a)** MIPAS (climatology for the period 2002–2011) **(b)** ECHAM5-HAMMOZ reference simulation between 8–23 km **(c)** same as figure **(b)** but from the surface. Latitude-altitude section of PAN (ppt) averaged for the monsoon season and 60–120° E **(d)** MIPAS climatology **(e)** PAN from ECHAM5-HAMMOZ reference simulation between 8–23 km, **(f)** same as figure **(e)** but from the surface. ECHAM5-HAMMOZ simulations are smoothed with averaging kernel of MIPAS. Wind vectors are indicated by black arrows in **(b)** and **(e)**. The vertical velocity field has been scaled by 300.

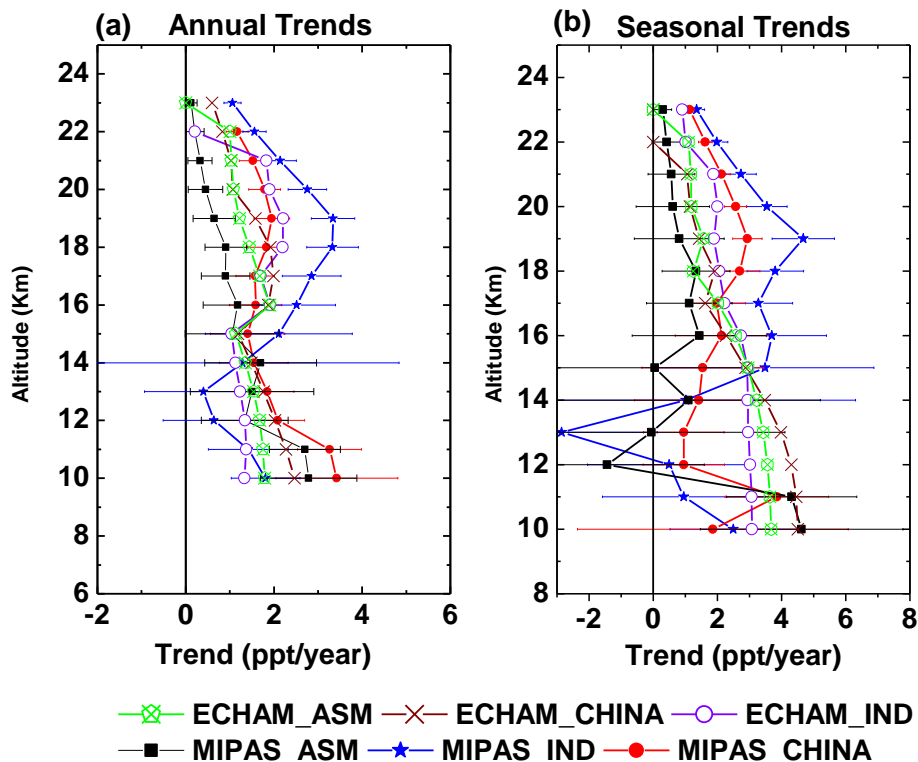


Figure 4. Vertical variation of trends obtained from monthly mean MIPAS-E PAN concentrations for the period 2002–2011 averaged and Ind38Chin73 simulations over the Asian summer monsoon region, China and India (a) annual trends (b) seasonal (June–September) trends.

[Title Page](#)
[Abstract](#)
[Introduction](#)
[Conclusions](#)
[References](#)
[Tables](#)
[Figures](#)
[◀](#)
[▶](#)
[◀](#)
[▶](#)
[Back](#)
[Close](#)
[Full Screen / Esc](#)
[Printer-friendly Version](#)
[Interactive Discussion](#)


Regional impacts

S. Fadnavis et al.

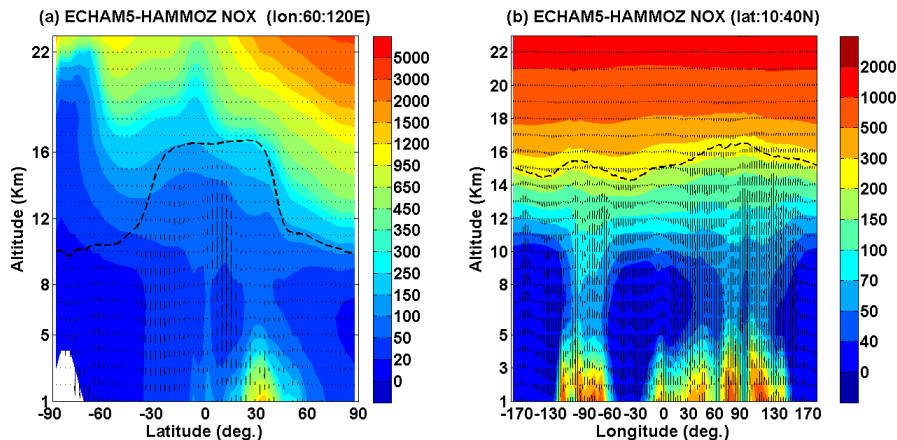


Figure 5. Latitude-altitude cross section of seasonal mean ECHAM5-HAMMOZ NO_x (ppt) **(a)** averaged for 60–120° E **(b)** averaged for 10–40° N. Wind vectors are indicated by black arrows. The vertical velocity field has been scaled by 300.

[Title Page](#)[Abstract](#)[Introduction](#)[Conclusions](#)[References](#)[Tables](#)[Figures](#)[◀](#)[▶](#)[◀](#)[▶](#)[Back](#)[Close](#)[Full Screen / Esc](#)[Printer-friendly Version](#)[Interactive Discussion](#)

[Title Page](#)
[Abstract](#)
[Introduction](#)
[Conclusions](#)
[References](#)
[Tables](#)
[Figures](#)

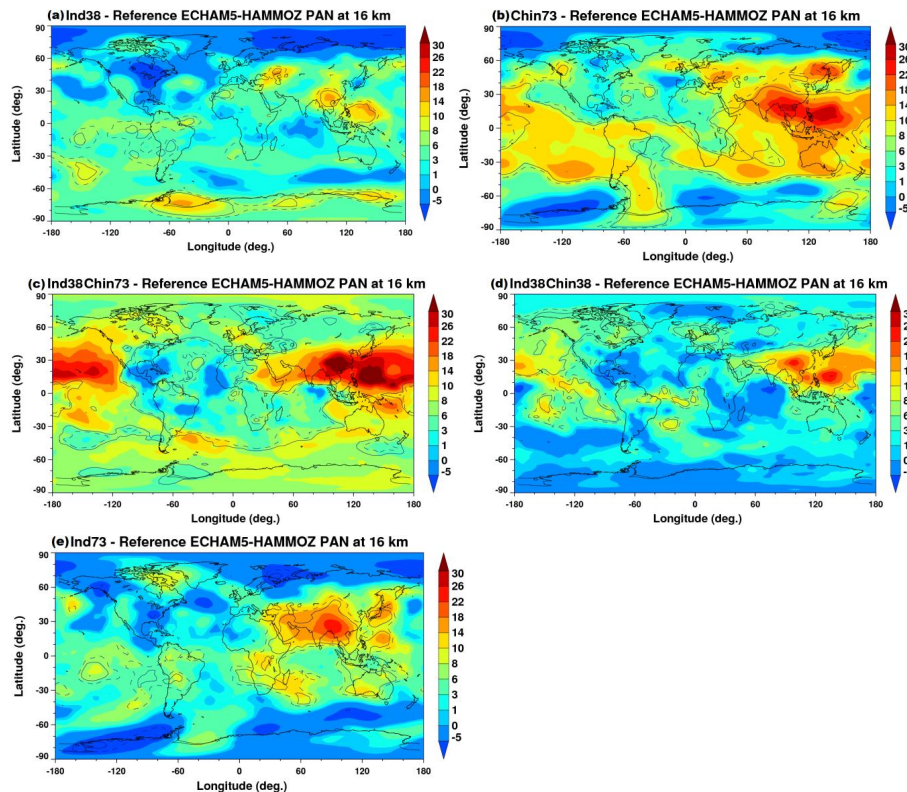
[Back](#)
[Close](#)
[Full Screen / Esc](#)
[Printer-friendly Version](#)
[Interactive Discussion](#)


Figure 6. Percentage change in ECHAM5-HAMMOZ PAN at 16 km, as obtained from (a) Ind38, (b) Chin73, (c) Ind38Chin73, (d) Ind38Chin38 and (e) Ind73 simulations. Solid black line indicates the 95 % Student's t test confidence interval while dashed line indicates 90 % confidence interval.

[Title Page](#)
[Abstract](#)
[Introduction](#)
[Conclusions](#)
[References](#)
[Tables](#)
[Figures](#)

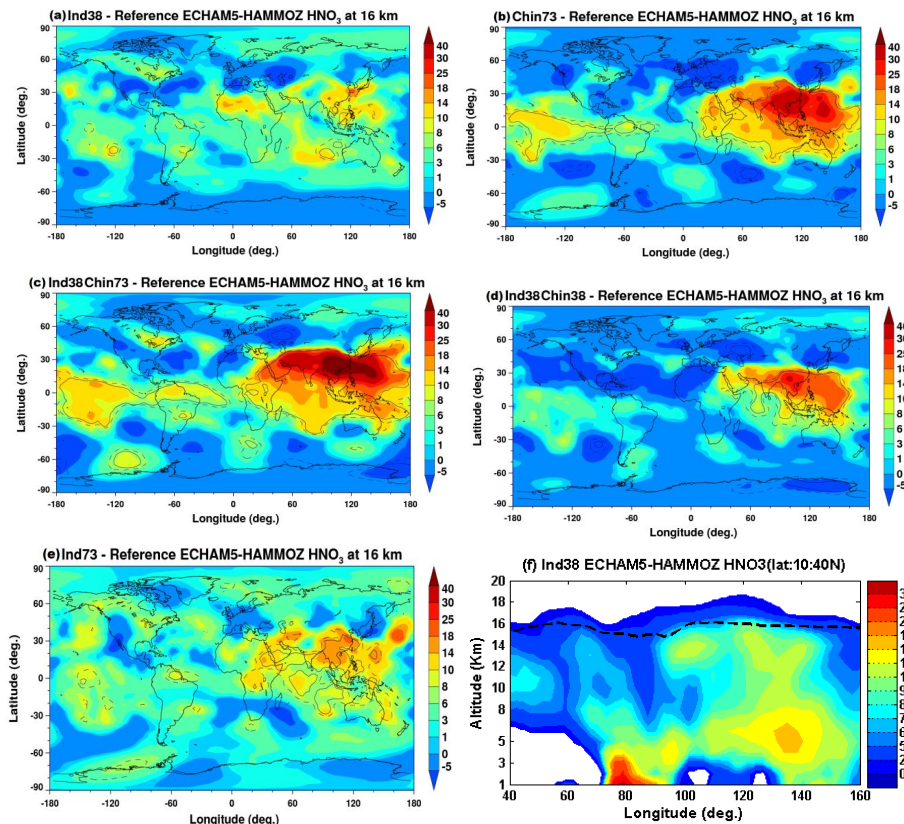
[Back](#)
[Close](#)
[Full Screen / Esc](#)
[Printer-friendly Version](#)
[Interactive Discussion](#)


Figure 7. Percentage change in ECHAM5-HAMMOZ HNO_3 at 16 km, as obtained from (a) Ind38, (b) Chin73, (c) Ind38Chin73, (d) Ind38Chin38 and (e) Ind73 simulations. Solid black line indicates the 95 % Student's t test confidence interval while dashed line indicates 90 % confidence interval (f) Longitude-altitude cross section (averaged over $0\text{--}40^\circ\text{N}$) of percentage change in HNO_3 for Ind38 simulation.

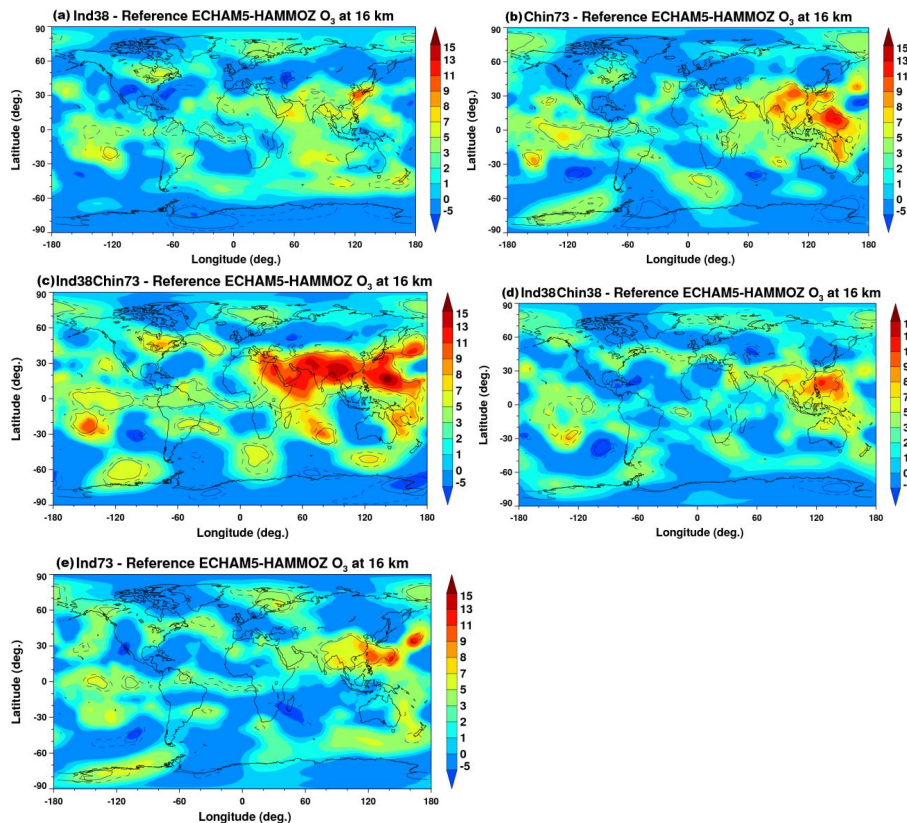
[Title Page](#)[Abstract](#)[Introduction](#)[Conclusions](#)[References](#)[Tables](#)[Figures](#)[Back](#)[Close](#)[Full Screen / Esc](#)[Printer-friendly Version](#)[Interactive Discussion](#)

Figure 8. Percentage change in ECHAM5-HAMMOZ ozone at 16 km, as obtained from (a) Ind38, (b) Chin73, (c) Ind38Chin73, (d) Ind38Chin38 and (e) Ind73 simulations. Solid black line indicates the 95 % Student's t test confidence interval while dashed line indicates 90 % confidence interval.